PHYSICAL REVIEW A VOLUME 24, NUMBER 6 DECEMBER 1981

Precision study of the $A\ ^2\Sigma^+$ state of the OH radical

Frederick Raab,* T. Bergeman, David Lieberman, and Harold Metcalf
Department of Physics, State University of New York at Stony Brook Stony Brook, New York 11794
(Received 21 May 1981)

We report precision measurements and calculations of several parameters of the $A\ ^2\Sigma^+$ state of the OH free radical. Data from quantum beats in the fluorescence of laser-excited molecules and direct optical spectroscopy have been combined to yield the following values for the parameters of our model Hamiltonian: $\gamma=6862(43)$ MHz, $b+c/3=774.1(0.4)$ MHz, $c=168.9(0.8)$ MHz, $g_r=0.002\,48(0.6)\mu_B$, and $g_A=0.0242(11)\mu_B$. Calculations that include coupling to the ground $X\ ^2\Pi$ states through rotational or spin-orbit interactions produce estimates of these parameters that agree very well for all except g_A.

I. INTRODUCTION

The OH free radical has attracted the interest of spectroscopists for over 50 years and has recently been the object of vigorously renewed study. The prominent $A\ ^2\Sigma^+$-$X\ ^2\Pi$ bands in the near uv were analyzed in the early days of quantum mechanics, and the definitive study of the optical spectrum was published by Dieke and Crosswhite[1] 20 years ago. In recent years, there has been increasingly precise data on the $X\ ^2\Pi$ ground state from infrared, microwave,[2] electron spin resonance,[3,4] and laser magnetic resonance[5] techniques, which have yielded fine-, hyperfine-, Stark-, and Zeeman-structure parameters to extremely high precision. Also the excited state, $A\ ^2\Sigma^+$ has been studied by level crossing[6,7] and double resonance[8–10] techniques, by laser-atomic beam resonance,[11] and by observation of the Stark effect in a high electric field.[12] Available A-state hyperfine parameters[11,13] have error limits of ± 2.0 MHz or more, which does not yet match the radiative linewidth of 0.24 MHz, as determined from numerous lifetime measurements. Also, previous to our work,[13,14] the A-state Zeeman effect has not been studied precisely enough to test terms beyond simple vector coupling formulas. "Doppler-free" precision was achieved in many of these measurements by using level crossing or rf techniques. The advent of tunable lasers operating in the 3000 A region near the principal $X \rightarrow A$ transition has resulted in enormous growth in the study of the excited states.[11,13–22]

A thorough understanding of the structure of OH is desirable for many reasons. First, it is found in many regions of outer space. The initial discovery of celestial OH was in the radio absorption by an intersteller cloud in Cassiopeia, and this was followed by the discovery of OH maser emission operating on a Λ doublet transition from a cloud in the Orion nebula. It has since been found as both absorber and maser in a large number of stellar atmospheres as well as interstellar clouds. Second, it is an important constituent in the earth's upper atmosphere. Although atmospheric infrared spectra (nightglow) had been studied for many years, in 1950 certain emissions were discovered by Meinel[23] to derive from vibrational transitions within the ground state of OH. Since then a large number of upper atmosphere studies have centered around OH. Third, a number of studies have shown[24] that its interaction with ozone is important to the formation of urban smog. OH has even been detected in the ambient atmosphere, although it is highly reactive. Fourth, it is formed copiously in any combustion process involving hydrogen, particularly fossil fuels. Its concentration and temperature may serve as possible probes for combustion diagnostics. Also, laser excitation of OH in flames could alter the burning efficiency or speed.

The present experiments demonstrate the utility of the laser-excited quantum-beat technique for precision measurements on molecular excited states. OH, like other hydrides, has the advantage of a relatively open rotational spectrum and a moderate partition function at room temperature, but our techniques are not limited to such molecules. We employ quantum beats to measure the Zeeman effect not only at low field (<25 G), giving g factors, but also in the vicinity of level crossings at higher field (200–800 G) so that these crossings are determined to a precision of one part in 10^4.

The experiments consist of pulsed laser excitation followed by recording of the temporal oscilla-

tions superposed on the exponentially decaying fluorescence in an applied magnetic field. The oscillation frequencies are equal to the energy intervals divided by Planck's constant, and thus provide a direct measurement of these intervals. We extract hyperfine-structure (hfs) parameters as well as g factors from the data.

II. EXPERIMENTAL

A. Sample

The experimental arrangement is shown in Fig. 1. Tank hydrogen is bubbled through water and dissociated in a 2450-MHz discharge ($\cong$40 W) and then flows about 1 m through carefully cleaned glass tubing to the interaction region. A 2-mm-diam orifice allows less than 1-m-Torr pressure in this region even though the discharge operates at about 1 Torr. The H atoms react with NO_2 gas, admitted through a glass "showerhead" arrangement, to form NO and OH: the OH rotational temperature is about 320 K. A 10-cm diffusion pump maintains vacuum and a removable liquid N_2 trap collects the residual NO_2.

B. Lasers

The OH is excited to the $A\ ^2\Sigma$ state by a pulse of light from a frequency-doubled, N_2 laser pumped dye laser. The home-built[25] nitrogen laser emits 500-kW, 8-nsec pulses of 3371 A light at about 10 Hz that are used to pump a tunable dye laser (6160 A) in an oscillator-amplifier configuration.[26] The

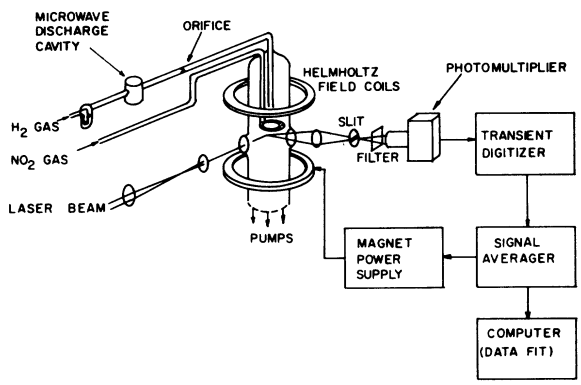

FIG. 1. Schematic diagram of experimental apparatus. Laser beam, detection direction, and magnetic field are mutually perpendicular. The OH is formed just above the glass ring "showerhead."

0.2-cm^{-1} bandwidth dye laser light is frequency doubled by an angle-tuned KDP crystal producing a 5-nsec, 200-W peak power pulse that is focused into a 1-mm-diam beam directed at the region where OH is produced. Most of the red light is filtered from the beam by a Corning glass no. 754 filter.

C. Magnetic field

An external magnetic field is applied by 40-cm-diam water-cooled Helmholtz coils that can produce nearly 1 kG (several kW power). The earth's field is carefully canceled by 40-cm square Helmholtz coils[27] and all magnetic materials are carefully excluded from the 40-cm cube inside the coils. The field homogeneity has been measured to better than one part in 10^4 over the viewing region and its absolute value measured with nuclear magnetic resonance (NMR) to better than one part in 10^5 at fields larger than 200 G. Its long-term stability is also about one part in 10^5. A precision shunt in series with the coils, immersed in 3 liters of oil for temperature stability, is used to determine the relative current and hence fields below 200 G. Careful shunt-voltage measurements and straight-line fits to NMR frequencies with both positive and negative fields (high enough for NMR) allow precision better than one part in 10^3 on these field determinations. Each quantum-beat data set includes independent field determinations by NMR (high field) or shunt-voltage measurements (low field).

D. Optics

The interaction region is imaged by a 3.5-cm-diam, 6.5-cm-focal-length quartz lens ($\Omega=0.03$ sr) with unit magnification, and a 10×2-mm slit parallel to the laser beam in the image plane passes fluorescent light through another Corning 754 filter to a 1P28 photomultiplier tube (PMT). The PMT is supplied with 1100 V and has appropriate capacitors on the last few dynodes to minimize the effects of saturation and to provide fast response. Its output is terminated in 50 Ω and is fed to a Biomation 8100 fast transient recorder.

E. Electronics

The transient recorder digitizes the PMT output from each laser pulse into 2000 channels (8 bits

each) separated by 10 nsec. Since the sampling time for each channel is only 2 nsec, a 10-nsec low-pass filter is placed at the input. The Biomation output is digitally transmitted to a Nicolet model 1072 which averages the output from many laser pulses. A typical data set consists of 30 min of data collection at a fixed field (about 20 000 laser pulses).

III. THEORY

A. Molecular structure

The structure of the $A\,^2\Sigma^+$ state studied here arises from the coupling of several angular momenta, and it is expected to exhibit pure Hund's case (b) behavior. It is customary to characterize various states by the rotational quantum number K and the angular momentum by $J=K\pm S$. This coupling is caused by an interaction $\gamma\vec{K}\cdot\vec{S}$ in each rotational state K with $\gamma\sim 7$ GHz (ρ doubling).

The $^2\Pi$ ground state is described by coupling intermediate between cases (a) and (b), with case (b) approached as J increases. Since the electronic spin $S=\frac{1}{2}$, there are two fine-structure states designated $\Pi_{3/2}$ and $\Pi_{1/2}$, respectively. Each rotational state is split into two states of the same J and opposite parity by the Λ-doubling interaction.

For OH it is customary to use the notation of Hund's case (b) for both the Σ and Π states. We shall follow the transition-labeling scheme employed by Dieke and Crosswhite[1] in all discussions below. Figure 2 indicates this structure, along with the standard notation and predicted transition intensities for the array of allowed transitions connecting a $K=4$ excited rotational state.

We shall momentarily ignore the hfs and consider the g factors for the $A\,^2\Sigma^+$ state. Since the magnetic moment associated with K is very small compared to a Bohr magneton, the g factor is dominated by the magnetic moment of the electron spin. For case (b) coupling, the g factor for a state of angular momentum J is given by

$$g_J=\frac{J(J+1)+S(S+1)-K(K+1)}{2J(J+1)}g_s\ , \qquad (1)$$

where g_s is the electronic-spin g factor. For $S=\frac{1}{2}$ and $g_s=2$, appropriate for a single unpaired electron, this reduces to

$$g_{K\pm 1/2}=\pm 1/(K+\tfrac{1}{2})\ . \qquad (2)$$

The hfs modifies the g factors. For a given J state and nuclear spin I, the g factors of the hyperfine components F are approximately

$$g_F=g_J\frac{F(F+1)+J(J+1)-I(I+1)}{2F(F+1)}\ , \qquad (3)$$

where $I=\frac{1}{2}$ for OH.

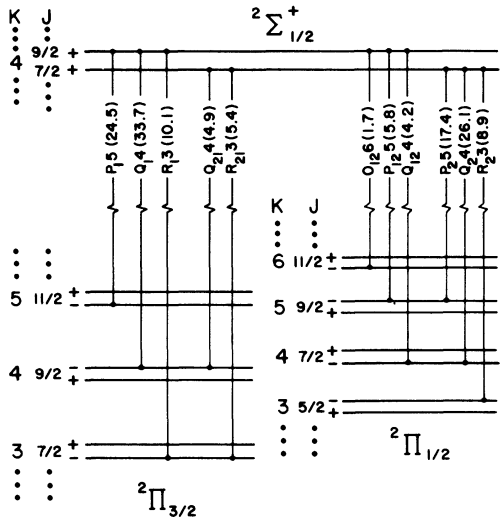

FIG. 2. Diagram of the transitions connecting the $K=4$ level of the $A\,^2\Sigma^+$ state with the ground state of OH. The hfs and Zeeman splitting are not shown. The notation is from Ref. 1.

B. First-order Hamiltonian

A more accurate description of the $A\,^2\Sigma$ state requires the careful construction of a molecular Hamiltonian. It may be written as the sum of five major terms

$$\mathcal{H}_0=\mathcal{H}_{\text{electron}}+\mathcal{H}_{\text{vibration}}\ , \qquad (4a)$$

$$\mathcal{H}_{\text{spin-orbit}}=A\vec{L}\cdot\vec{S}\ , \qquad (4b)$$

$$\mathcal{H}_{\text{rotation}}=B_r(\vec{K}-\vec{L})^2=B_r(\vec{K}^2+\vec{L}^2-2\vec{K}\cdot\vec{L})\ , \qquad (4c)$$

$$\mathcal{H}_{\text{hfs}}=\mathcal{H}_{\text{Fermi contact}}+\mathcal{H}_{\text{dipole-dipole}}$$
$$\equiv b\vec{I}\cdot\vec{S}+cI_zS_z\ , \qquad (4d)$$

and

$$\mathcal{H}_Z=\mathcal{H}_{el}+\mathcal{H}_{\text{nucl. spin}}+\mathcal{H}_{\text{nucl. rot.}}$$
$$=(g_s\mu_B\vec{S}+\mu_B\vec{L}-g_I\mu_N\vec{I}-g_{Nr}\mu_B\vec{K})\cdot\vec{B}\ . \qquad (4e)$$

Here $\mathcal{H}_0$ defines the energy of the particular state but plays no other role in our experiments; the next two terms have their conventional meaning.

$\mathcal{H}_{\text{hfs}}$ has been calculated by Frosch and Foley[28]

and its matrix elements have been evaluated by Radford.[29] b contains the Fermi-contact term and part of the dipole-dipole term; the rest of this latter term comprises c. The matrix elements, diagonal in K and M_F, are

$$\langle K,J=K\pm\tfrac{1}{2}\,|\,\mathscr{H}_{\rm hfs}\,|\,K,J=K\pm\tfrac{1}{2}\rangle = V[\pm b + c/(2J+1\pm1)]\,, \tag{5a}$$

$$\langle K,J=K\pm\tfrac{1}{2}\,|\,\mathscr{H}_{\rm hfs}\,|\,K,J=K\mp\tfrac{1}{2}\rangle = W[b+c/2]\,, \tag{5b}$$

$$V=\frac{[F(F+1)-I(I+1)-J(J+1)]}{2(2K+1)}\,, \tag{5c}$$

$$W=[(F+K-I+\tfrac{1}{2})(F+I-K+\tfrac{1}{2}) \times(F+K+I+\tfrac{3}{2})(K+I-F+\tfrac{1}{2})]^{1/2}\,. \tag{5d}$$

The first term of $\mathscr{H}_z$ contains the ordinary Zeeman effect of an electron spin in a magnetic field and can be evaluated using standard angular momentum recoupling formalism.[30] Our case (b) coupling scheme is $((K,S)J,I)F,M_F\equiv\beta$, where $S=I=\frac{1}{2}$ for doublet states of OH. The projection of K on the internuclear axis is zero for Σ states. Thus for a $\vec{B}$ field (do not confuse the $\vec{B}$ field with the rotation constant B_r) in the z direction

$$\langle {}^2\Sigma^+\beta\,|\,g_s\mu_B\vec{S}\cdot\vec{B}\,|\,{}^2\Sigma^+\beta'\rangle = g_s\mu_B B_z Q_{SB} J_3 W(JJ'FF';1I)W(SSJJ';1K)\,, \tag{6a}$$

$$Q_{SB}=(-1)^{F-I+S-K+1}[S(S+1)(2S+1)(2F'+1)(2J+1)(2J'+1)]^{1/2}\,, \tag{6b}$$

$$J_3=\langle F'1M_F0\,|\,FM_F\rangle\,, \tag{6c}$$

where the W's are Wigner coefficients, J_3 is a Clebsch-Gordan coefficient $\langle J_1J_2M_1M_2\,|\,JM\rangle$, and $g_S=2.002\,32$. Relativistic effects for g_S in the OH $X\,^2\Pi$ ground state have been estimated by Veseth[31] from an expression $\langle T\rangle/mc^2$ to be 1.3×10^{-4}. This correction would be slightly smaller for an excited state and is at the limit of precision of our data. These matrix elements are diagonal in K and M_F. There are no first-order contributions to the Hamiltonian matrix from the $\vec{L}\cdot\vec{B}$ terms of Eq. (4e).

The third term in the Zeeman Hamiltonian arises from the interaction of the nuclear spin with the magnetic field and is evaluated in much the same way as the first term. The matrix elements, also diagonal in K and M_F, are

$$\langle {}^2\Sigma^+\beta\,|\,-g_I\mu_N\vec{I}\cdot\vec{B}\,|\,{}^2\Sigma^+\beta'\rangle = g_I\mu_N B_z Q_{IB} J_3 W(IIFF';1J)\delta_{JJ'}\,, \tag{7a}$$

$$Q_{IB}=(-1)^{F'+I-J}[I(I+1)(2I+1)(2F'+1)]^{1/2}\,. \tag{7b}$$

The fourth term arises from the magnetic moment associated with the rotating nuclei. It has similar matrix elements given by

$$\langle {}^2\Sigma^+\beta\,|\,-g_{Nr}\mu_B\vec{K}\cdot\vec{B}\,|\,{}^2\Sigma^+\beta'\rangle = g_{Nr}\mu_B B_z Q_{KB} J_3 W(JJ'FF';1I)W(KKJJ';1S)\,, \tag{8a}$$

$$Q_{KB}=(-1)^{J+J'-I-S+K+F}[(2J+1)(2J'+1)K(K+1)(2K+1)(2F'+1)]^{1/2}\,. \tag{8b}$$

Here g_{Nr} is calculated from the motion of the bare rotating nuclei,

$$g_{Nr}=m(Z_{\rm O}M_{\rm H}^2+Z_{\rm H}M_{\rm O}^2)/M_{\rm O}M_{\rm H}(M_{\rm O}+M_{\rm H})\,, \tag{9}$$

where m is the electron mass, O and H refer to oxygen and hydrogen, and Z and M are charges and masses, respectively.

Each of these terms is diagonal in I and Λ as well as in K and M_F. It is therefore convenient to discuss the Hamiltonian matrix in terms of 4×4 submatrices having $J=K\pm\frac{1}{2}$ (for $S=\frac{1}{2}$) and $F=J\pm\frac{1}{2}$ (for $I=\frac{1}{2}$), but diagonal in the quantities K, S, Λ, I, and M_F.

C. Second-order terms

In addition to the contributions of Eqs. (5)—(8) above, there are other terms in the Hamiltonian matrix relevant to our measurements. These arise from the spin-orbit and rotation terms that are off diagonal in Λ and typically involve coupling to the ground electronic state $X\,^2\Pi$. Diagonalizing a Hamiltonian matrix with terms coupling such widely separated states is an unwieldy calculation, but may be approximated by a

method developed by Van Vleck and described by Jordahl.[32] The Van Vleck transformation produces matrix elements that have the form of second-order perturbation terms.

For example, we consider the term $-2B_r\vec{K}\cdot\vec{L}$ in Eq. (4c) and the $A\vec{L}\cdot\vec{S}$ term of Eq. (4b). The coupling of these through the ground Π state gives rise to the well-known ρ-doubling term usually written as $\gamma\vec{K}\cdot\vec{S}$. To introduce this term into the Hamiltonian we consider a second-order perturbative sum, as prescribed by the Van Vleck transformation, over the $^2\Pi$ states:

$$-4\langle {}^2\Sigma^+ v\beta \,|\, (B_r\vec{K}\cdot\vec{L})(A\vec{L}\cdot\vec{S}) \,|\, {}^2\Sigma^+ v\beta'\rangle = -4\sum_\alpha \frac{\langle {}^2\Sigma^+ v\beta \,|\, B_r\vec{K}\cdot\vec{L} \,|\, \eta^2\Pi v''\beta''\rangle\langle \eta^2\Pi v''\beta'' \,|\, A\vec{L}\cdot\vec{S} \,|\, {}^2\Sigma^+ v\beta'\rangle}{E({}^2\Sigma^+ v) - E(\eta^2\Pi v'')} , \tag{10}$$

where the number v denotes the vibrational state and the quantum numbers α of the sum are η, v'', K'', J'', F''.

The matrix elements of $\vec{K}\cdot\vec{L}$ and of $\vec{L}\cdot\vec{S}$ are

$$\langle \eta^2\Pi v''\beta'' \,|\, B_r\vec{K}\cdot\vec{L} \,|\, {}^2\Sigma^+ v\beta\rangle = \langle K\,101 \,|\, K''1\rangle\langle 1||T^1_1(L)||0\rangle\langle v'' \,|\, B_r \,|\, v\rangle[2K(K+1)]^{1/2}\delta_{FF''}\delta_{JJ''}\delta_{KK''} \tag{11}$$

and

$$\langle \eta^2\Pi v''\beta'' \,|\, A\vec{L}\cdot\vec{S} \,|\, {}^2\Sigma^+ v\beta\rangle = \langle K\,101 \,|\, K''1\rangle\langle 1||AT^1_1(L)||0\rangle\langle v'' \,|\, v\rangle Q_{LS} W(SSK''K;1J'')\delta_{FF''}\delta_{JJ''} , \tag{12a}$$

$$Q_{LS} = (-1)^{J''-S-K}[2S(S+1)(2S+1)(2K+1)]^{1/2} . \tag{12b}$$

Because parity eigenfunctions for the $^2\Pi$ state are linear combinations $(|\Lambda=1\rangle \pm |\Lambda=-1\rangle)/\sqrt{2}$, the elements given above are $\sqrt{2}$ times the element simply for $\Lambda=1$. Substituting Eqs. (11) and (12) into Eq. (10) produces an expression proportional to $\vec{K}\cdot\vec{S}$, the ρ doubling. To estimate the coupling constant γ, we assume that coupling only with the ground $X\,^2\Pi$ state is significant. Parameters for the A-X interaction needed for this model both here and below may by obtained from Λ-doubling and Zeeman-effect (EPR) measurements within the $X\,^2\Pi$ state. γ then arises from a sum over vibrational levels of the X state

$$\gamma_v = -4\langle 0||T^1_{-1}(L)||1\rangle\langle 1||T^1_1(AL)||0\rangle \sum_{v''} \frac{\langle v \,|\, B_r \,|\, v''\rangle\langle v'' \,|\, v\rangle}{E({}^2\Sigma^+ v) - E({}^2\Pi v'')} , \tag{13}$$

where we have assumed that the electronic factors are independent of r. This sum is identical except for a sign to the theoretical expression for the Λ-doubling constant p in the $^2\Pi$ state, and that for p the summation is over v rather than v''. A comparison of γ and p values provides a test of the two-state model. To a first approximation, $\gamma=p$, but when the appropriate sums over v or v'' are computed (see the Appendix) one obtains $\gamma=0.9325p$.

A recent comprehensive fit to optical and microwave data yielded[33]

$$p = 0.2348 \text{ cm}^{-1} = 7039 \text{ MHz} , \tag{14a}$$

and hence

$$\gamma = 0.2190 \text{ cm}^{-1} = 6564 \text{ MHz} . \tag{14b}$$

We next consider a small correction term involving $\mu_B\vec{L}\cdot\vec{B}$ and $A\vec{L}\cdot\vec{S}$. The $\vec{L}\cdot\vec{B}$ part represents a slight coupling of the electron spin perpendicular to the internuclear axis and resembles a term g_A in Veseth's recent papers.[31] To introduce this term into the Hamiltonian, we again consider a second-order perturbation sum over $^2\Pi$ states:

$$\langle {}^2\Sigma^+ v\beta \,|\, (\mu_B\vec{B}\cdot\vec{L})(A\vec{L}\cdot\vec{S}) \,|\, {}^2\Sigma^+ v\beta'\rangle = \sum_\alpha \frac{\langle {}^2\Sigma^+ v\beta \,|\, \mu_B\vec{B}\cdot\vec{L} \,|\, \eta\,{}^2\Pi v''\beta''\rangle\langle \eta\,{}^2\Pi v''\beta'' \,|\, A\vec{L}\cdot\vec{S} \,|\, {}^2\Sigma^+ v\beta'\rangle}{E({}^2\Sigma^+ v) - E(\eta^2\Pi v'')} . \tag{15}$$

This term is evaluated by substituting

$$\langle {}^2\Sigma^+ v\beta \,|\, \vec{B}\cdot\vec{L} \,|\, \eta^2\Pi v''\beta''\rangle = B_z Q_{BL} J_3 W(KK''JJ'';1S)\langle K''11-1 \,|\, K0\rangle\langle 0||T^1_{-1}(L)||1\rangle\langle v \,|\, v''\rangle \ , \tag{16a}$$

$$Q_{BL} = (-1)^{K''-S+J+J''+F-I} W(JJ''FF'';1I)[2(2F''+1)(2J+1)(2J''+1)(2K''+1)]^{1/2} , \tag{16b}$$

and the $A\vec{L}\cdot\vec{S}$ matrix elements of Eq. (12). A sum over K'' as well as over v'' remains in Eq. (15).

These terms involving $\vec{B}\cdot\vec{L}$ and $A\vec{L}\cdot\vec{S}$ may be related to a parameter that we designate g_A (Ref. 31):

$$g_A = 4\langle 0||T^1_{-1}(L)||1\rangle\langle 1||T^1_1(AL)||0\rangle \sum_{v''} \frac{|\langle v \,|\, v''\rangle|^2}{E({}^2\Sigma^+ v) - E({}^2\Pi v'')} \ . \tag{17}$$

From values of the coupling elements between $A\,^2\Sigma^+$ and $X\,^2\Pi$ given in the Appendix, we obtain $g_A = -1.30\times 10^{-2}$. This parameter is similar to but not identical with the parameter for Zeeman effect anisotropy ($\delta g = g_\perp - g_{||}$) used in our preliminary report.[13]

Similarly, there is a contribution to g_r from the electrons arising from a combination of Hamiltonian terms $\vec{B}\cdot\vec{L}$ and $-2B_r\vec{L}\cdot\vec{K}$. There is no contribution from $\vec{B}\cdot\vec{L}$ strictly within the $A\,^2\Sigma^+$ state because the diagonal elements of orbital angular momentum are zero in the nuclear frame and hence also in the space-fixed frame.[31] Hence we are concerned with second-order perturbation terms coupling to the $^2\Pi$ states:

$$-g_{\rm er}\mu_\beta \vec{K}\cdot\vec{B} = -4 \sum_{\eta v''} \frac{\langle {}^2\Sigma^+ v\beta \,|\, \vec{B}\cdot\vec{L} \,|\, \eta^2\Pi v''\beta''\rangle\langle \eta^2\Pi v''\beta'' \,|\, B_r\vec{L}\cdot\vec{K} \,|\, {}^2\Sigma^+ v\beta'\rangle}{E({}^2\Sigma^+ v) - E(\eta\,{}^2\Pi v'')} \ . \tag{18}$$

The appropriate matrix elements have been given in Eqs. (11) and (16). Substitution of these expressions into Eq. (18) produces a term that looks very much like the rotational part of $\mathscr{H}_z$ in Eq. (4e), but arises solely from the electrons. This electron contribution to the rotational g factor from $X\,^2\Pi$ is

$$g_{\rm er} = 4\langle 0||T^1_{-1}(L)||1\rangle\langle 1||T^1_1(L)||0\rangle \sum_{v''} \frac{\langle v \,|\, v''\rangle\langle v'' \,|\, B_r \,|\, v\rangle}{E({}^2\Sigma^+ v) - E({}^2\Pi v'')} \ . \tag{19}$$

The parameters given in the Appendix are again substituted and we find $g_{\rm er} = 1.89\times 10^{-3}$. Evaluation of Eq. (9) gives $g_{Nr} = 0.53\times 10^{-3}$, so that our "theoretical" value is

$$g_r = g_{\rm er} + g_{Nr} = 2.42\times 10^{-3} \ .$$

There are many other nonzero matrix elements in the Hamiltonian that might be considered as well. All the second-order terms involving the Hamiltonian terms of Eq. (4a) are zero. Those involving the same term twice (nonmixing) provide overall shifts of an entire manifold of levels. Of the remaining six mixing terms, three have been discussed above and two of the others involving the hfs [Eq. (4d)] are extremely small. The last one, the hfs-rotation coupling, is described by a term proportional to $\vec{I}\cdot\vec{J}$ and has been explored in our least-squares adjustment program described below. Its coupling constant is very small, estimated to be less than 0.5 MHz in magnitude.

D. Energy levels

The Hamiltonian matrix elements above are those of Refs. 34 and 35 except for the term in g_A, which resembles a similar term in Ref. 31. The g_r and g_A terms have not previously been measured in a $^2\Sigma$ state. We diagonalize the 4×4 matrix with second-order terms at each value of the magnetic field where we have taken data. At low fields we calculate the energy difference between all pairs of Zeeman sublevels with M_F different by 2 in a particular state $|KJF\rangle$, average them, and divide by $2\mu_B B$ to obtain the theoretical g factor. In the weak fields we use, the effect of hfs uncoupling from the mixing of F states is negligibly small and the error we make by averaging is much less than our experimental uncertainty.

The resulting g_F values are given approximately by Eq. (3), but there are contributions of the order of 1% from the off-diagonal hfs matrix elements, the nuclear Zeeman effect, the rotational g factor, and the anisotropic g factor. Each of these small contributions has a different dependence on the molecular angular momenta, and our data are sufficiently precise to distinguish them from one another.

E. Quantum beats

A perturbative model of quantum beats observed by fluorescence has been described[36] and applied to

the OH molecule[13,14] by us. The general features that we assume in order to adopt that model in this work are that the molecules are excited by a temporally square, spectrally white pulse, and that the observation aperture is also temporally square. Equation (4) of Ref. 36, reproduced below, shows that the rate of fluorescence $R(T)$ is

$$R(T)\propto \sum_{\substack{\mu\mu' \\ mm'}} f_{\mu m}f_{m\mu'}g_{\mu' m}g_{m'\mu}[e^{-\Gamma T}/(\Gamma^2+\omega^2)^2]$$
$$\times\{(\omega^2-\Gamma^2+2i\omega\Gamma)[\cos\omega T+e^{-\Gamma\tau}\cos\omega(T+\tau)-e^{-\Gamma\theta}\cos\omega(T+\theta)-e^{-\Gamma\delta}\cos\omega(T+\delta)]$$
$$+[2\omega\Gamma-i(\omega^2-\Gamma^2)][\sin\omega T+e^{-\Gamma\tau}\sin\omega(T+\tau)-e^{-\Gamma\theta}\sin\omega(T+\theta)-e^{-\Gamma\delta}\sin\omega(T+\delta)]\}\,, \tag{20}$$

where the f's and g's are electric-dipole matrix elements between the Π states denoted by m and the Σ states denoted by μ, ω is the energy separation between sublevels μ and μ' of the Σ state, θ is the laser pulse duration, δ is the detector's temporal resolution, and $\tau=\theta+\delta$.

We separate the time dependence of Eq. (20) using trigonometric identities, collect terms in $\cos\omega T$ and $\sin\omega T$, and find

$$R(T)\propto \sum_{\substack{\mu,\mu' \\ m,m'}} f_{\mu m}f_{m\mu'}g_{\mu' m'}g_{m'\mu}\frac{e^{-\Gamma T}}{(\Gamma^2+\omega^2)^2}[(\omega^2-\Gamma^2)+2i\omega\Gamma]\{[\alpha(\omega)-i\beta(\omega)]\cos\omega T-[\beta(\omega)+i\alpha(\omega)]\sin\omega T\}\,, \tag{21a}$$

where

$$\alpha(\omega)=(1+e^{-\Gamma\tau}\cos\omega\tau-e^{-\Gamma\theta}\cos\omega\theta-e^{-\Gamma\delta}\cos\omega\delta)\,, \tag{21b}$$

$$\beta(\omega)=(e^{-\Gamma\tau}\sin\omega\tau-e^{-\Gamma\theta}\sin\omega\theta-e^{-\Gamma\delta}\sin\omega\delta)\,. \tag{21c}$$

Here $\alpha(\omega)$ and $\beta(\omega)$ are constants determined by the timing parameters which affect the amplitude and phase of the beat but do not affect the observed frequency.

Although each term in the sum over μ,μ' is complex, the imaginary part sums to zero and the overall rate is necessarily real. It is helpful to separate the time dependence of this expression into real and imaginary components:

$$R(T)=\sum_{m,m'}\sum_{\mu,\mu'} f_{\mu m}f_{m\mu'}g_{\mu' m'}g_{m'\mu}\frac{e^{-\Gamma T}}{(\Gamma^2+\omega^2)^2}$$
$$\times(\{(\omega^2-\Gamma^2)[\alpha(\omega)\cos\omega T-\beta(\omega)\sin\omega T]+2\omega\Gamma[\alpha(\omega)\sin\omega T-\beta(\omega)\cos\omega T]\}$$
$$+i\{2\omega\Gamma[\alpha(\omega)\cos\omega T-\beta(\omega)\sin\omega T]-(\omega^2-\Gamma^2)[\alpha(\omega)\sin\omega T+\beta(\omega)\cos\omega T]\})\,. \tag{22}$$

Since $\alpha(\omega)$ and $\beta(\omega)$ are, respectively, even and odd functions of ω, the real part of the time dependence is even in ω, and the imaginary part is odd. When the product of the transition matrix elements is real, the imaginary part of the time dependence sums to zero and the line shape is an even function of ω. This is the case for the orthogonal geometry used in our experiments.

For the $A\,^2\Sigma$ state of OH, Γ is about 0.22 MHz. In our experiments θ is about 5 nsec and δ is about 10 nsec. We therefore expand the functions in Eq. (21) above, keeping terms to second order, and find $\alpha(\omega)\simeq\delta\theta(\Gamma^2-\omega^2)$, $\beta(\omega)\simeq-2\omega\Gamma\theta\delta$, and

$$R(T)\simeq-\theta\delta e^{-\Gamma T}\sum_{mm'\mu\mu'} f_{\mu m}f_{m\mu'}g_{m\mu'}g_{\mu' m'}e^{-i\omega T}\,. \tag{23}$$

It is now clear that geometrical and/or polarization imperfections affect only the magnitude and

phase of the signal through the f's and g's but not the oscillation frequency.

A related calculation shows that spectral structure in the exciting light, spectral sensitivity of the detector, or temporal structure in the detector aperture or laser pulse will affect the magnitude of the integrals I_1 and I_2 of Ref. 36, but not the modulation frequency of the signal. Quantum-beat spectroscopy is uniquely immune from the ill effects of a large number of perturbations. It is very tolerant of a variety of simplifying assumptions about the experimental conditions.

The observed modulation of the fluorescence arises from interference of the probability amplitudes for the different paths taken by single OH molecules in their transitions from initial to final states. This interference appears when either the $^2\Sigma^+$ sublevels are not resolved in the molecule ($\Gamma > \omega_{\mu\mu'}$) or when the spectral profile of the exciting light has a *homogeneous* width $\Delta\omega > \omega_{\mu\mu'}$. Although the $^2\Sigma^+$ sublevels are generally well resolved in our experiments, the 5-nsec laser pulses are Fourier-transform broadened (homogeneous) to 30 MHz, much larger than $\omega_{\mu\mu'}$. On the other hand, the Doppler broadening of the absorption ($\omega_D > \omega_{\mu\mu'}$) is *inhomogeneous* and therefore cannot produce interference from a narrow-band excitation even though it prevents optical resolution of the hyperfine and Zeeman splitting.

The signals we observe derive from one or a few particular terms μ and μ' in a sum of a very large number of terms. Unlike atomic quantum-beat signals described by sums of 10 or 20 terms, these can easily have several hundred. A particular K state of $A\ ^2\Sigma$ can decay to ground states of $K+1$, K, or $K-1$ (P, Q, and R branches) which are generally not available in atomic cases. Furthermore, the large values of total angular momentum permit very high multiplicity ($F=6$ has 13 sublevels and 169 pairs of levels) and therefore considerable dilution of the high-field level-crossing signals. Finally, there are many cases where the signals from two or three of these branches cancel significantly as discussed in some detail in Ref. 8, thereby weakening the signal/background ratio substantially. We have used a computer program based on simple angular momentum matrix elements to estimate the relative strength of various signals and to guide us in our choice of high-field level crossings. These calculations agree with our observations of a few percent modulation of the fluorescence near zero field and as little as 0.1% modulation near the high-field crossings.

IV. DATA PROCESSING AND UNCERTAINTIES

A. Data processing

Each data set is transmitted to our computer and the dominating exponential decay is removed by division with another data set taken at a field where there is no signal. For the low-field data this normalizing set is taken at about 150 G, and for the high-field data it is taken 150 G away from the crossing. In each case the oscillations are at a frequency too high for the bandwidth of our detection system. This normalization signal is not exactly exponential because of a variety of problems associated with finite sample size, viewing region size, and laser-beam diameter.[37] We cannot use the decay to determine the lifetimes more accurately than existing published values.[38]

After dividing out the quasiexponential decay, each data set is fit with an oscillatory signal containing the (high-field) or two (low-field) frequencies. We have tried adding additional frequencies to the fit to look for extraneous effects and have found none. We also Fourier transform the data to search for artifacts but none appear. Furthermore, we have generated artificial data sets, with appropriate noise, containing extra frequencies and found that both the Fourier transform and the fitting program find and fit them. For these and other reasons we are confident that our program returns accurate values of the fitted parameters and statistically significant values of the uncertainties associated with each of them. The χ^2 values returned by the fits are almost always of order unity.

B. Low-field data

Each $|K,J\rangle$ level is split by the hfs into two states of $F=J\pm I$, having g factors given approximately by Eq. (3), and separated by much less than our laser linewidth (see Fig. 3). At low fields we see quantum-beat signals at two frequencies which add together giving a "beat" pattern as shown in Fig. 4(a). The beats spread and shift as the magnetic field is varied. Figure 4(b) shows the data from one of these signals after normalization for the decay. The solid line is a fit to this data of two oscillations with different amplitude, frequency, and phase. We have measured the 22 g factors of 11 such hyperfine pairs with $K=1$ to 6 as well as the ratios of the g factors of each pair. The measured values of the ratios are independent of

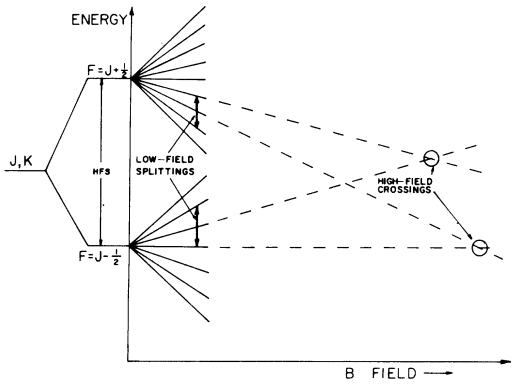

FIG. 3. Zeeman energy levels of a particular J,K state showing $F=J\pm\frac{1}{2}$ hyperfine levels. The other component of the ρ doublet is separated by about 20 times the diagram height. The laser width is about three times the diagram height.

the field calibration and most of them are accurate to about 0.1%.

C. High-field data

At high fields, we measured quantum-beat frequencies in the vicinity of several level crossings (see Fig. 5). Each data set is normalized for the decay as above, and a single frequency is fitted. The field value corresponding to zero frequency gives the crossing field to about 0.01% (100 parts in 10^6), and the Zeeman-Hamiltonian (g factors) allows extrapolation to the zero-field splitting. The hfs parameters b and c may be estimated from this splitting. We have made these measurements on two level crossings in different rotational states.

D. Optical measurements

Although our quantum-beat data are sufficiently sensitive to determine γ, the ρ-doubling constant, the result is only accurate to about 10%. Furthermore the determination may be subject to the influence of terms not yet included in the Hamiltonian. We have therefore made 14 direct optical measurements of the ρ splitting in the $K=1-5$ levels, each accurate to about 0.015 $cm^{-1}=450$ MHz, and used the average 6879 ± 75 MHz in the self-consistent analysis. Varying it by 75 MHz makes significant changes. This value is near the average of an optical measurement[1] ($\gamma=6732$ MHz) and a beam-laser measurement[11] [$\gamma=7130$ (30) MHz].

These measurements are made sweeping the laser frequency with a clock motor rotating the grating,

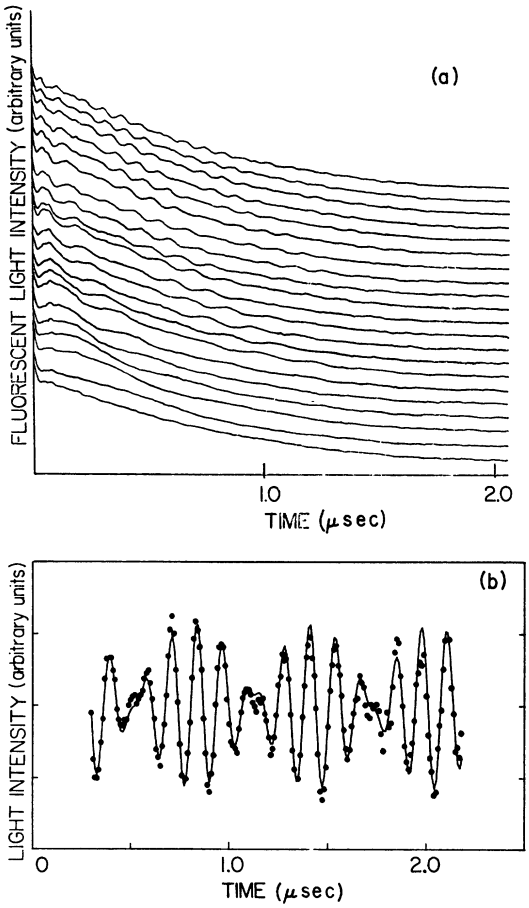

FIG. 4. (a) Fluorescent light intensity as a function of time for the $K=4$ rotational sublevel of the $A\,^2\Sigma^+$ state for different applied magnetic fields. The fields range from 20 G (top curve) to 0 G (bottom curve) in increments of 1 G. (b) One of these curves with the dominant decaying behavior divided out (see text). The uncertainties in the data points (depicted as dots) are on the order of the dot size. The solid line is fitted using a model of oscillations at two nearly equal frequencies.

and recording the fluorescence. Although we can make approximate wavelength measurements with a monochromator, the molecule itself provides a much more accurate calibration. We use the values of the rotational constant determined optically[1] to provide a long scale for the strip chart recording of the fluorescent spectrum (about 5 m of paper), and then measure the separation between peaks of the ρ doublet directly. A typical half-meter section of strip chart containing one doublet is shown in Fig. 6. We determine the scale accuracy to less than 1% but the peak separation to only about 5% resulting in a 500-MHz uncertainty for each frequency.

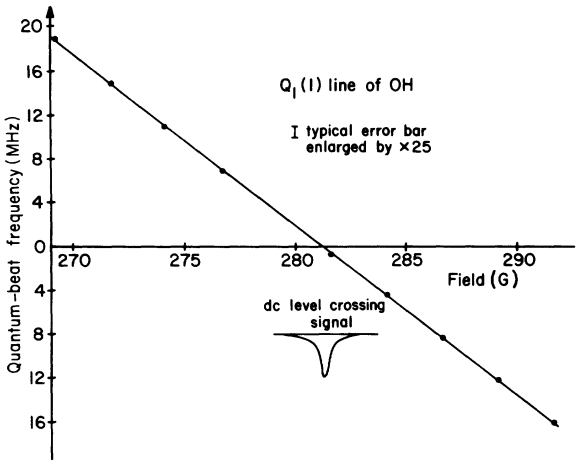

FIG. 5. Quantum-beat frequency vs magnetic field.

E. Data analysis

The data-fitting programs discussed above extract a frequency or energy interval between a particular, well-defined pair of levels at a particular field from each data set. We diagonalize the 4×4 matrix described above for each particular set of quantum numbers at the appropriate field, using trial values of the parameters, and compare the experimental values of the resulting energy intervals in a least-squares-fit program that adjusts the parameters for the best fit to all these measured frequencies. The g factors are calculated from the field and frequency as described in Sec. III D above. Each experimental number is weighted by the uncertainty returned by the data-fitting program.

The result is shown in Table I. The uncertainties associated with experimental numbers derive from the statistical scatter from the fitting program only, and do not reflect the systematic errors described below. The uncertainties associated with the theoretical values reflect only the statistical scatter in the determination of the parameters. The agreement between our model and our measurements is excellent, as shown in Fig. 7.

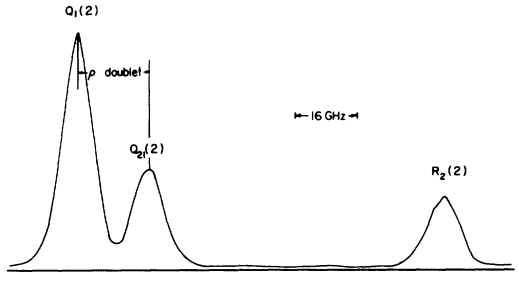

FIG. 6. A 0.5-m section of strip chart showing one ρ doublet and another line. The large interval was typical of the type used to determine the wavelength scale to about 0.5 GHz. The signal-to-noise ratio is very high.

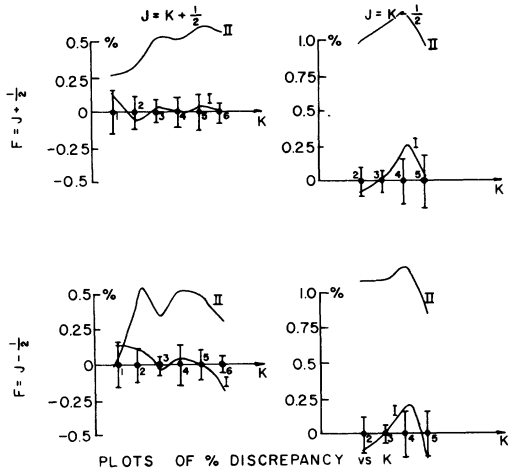

FIG. 7. Plots comparing theoretical and experimental g factors for the four cases $J=K\pm\frac{1}{2}$ and $F=J\pm\frac{1}{2}$. Direct plots of the g factors would have discrepancies too small to see. These show the percentage difference from the data that therefore appear on the axis. Curve I is the result of the best fit to the parameters as listed in Table II. Curve II is the result from fixing g_A at $-0.0066\,\mu_B$. Fixing it at the theoretical -0.013 would compress the scale too much.

F. Systematic errors

Most of our measurements consist of determination of a field and a frequency, and the systematic errors associated with each of these are very small compared with our statistical uncertainties. At high fields we use a marginal oscillator NMR scheme to determine the field to 10 ppm. These measurements were made before and after each data set was taken. The field was mapped and found to be homogeneous, repeatable, and stable. A directionally sensitive Hall probe was used with Helmholtz coils to reduce the horizontal components of the earth's field to less than 0.05 G.

The low-field measurements depended on calibration of an oil-immersed precision shunt in series with the coils, whose voltage was measured with a five-digit DVM. The shunt was calibrated at fields from 150–600 G (both positive and negative) where the NMR could be used to establish a field versus voltage curve. This was straight to better than one part in 10^4 and passed directly through the ambient laboratory field at zero shunt voltage.

TABLE I. The results of the least-squares program that adjusts the parameters for best fit to the frequencies extracted from the data by the data-fitting program. The parameters are then used to calculate each frequency or g factor and the results are presented for comparison with the data. We have presented the "best-fit" parameters, and then changed g_A to its theoretical value and fixed it there for another fit, and show the results of both for comparison.

			g factors (low field)				Frequencies (high field)			
				Theory	Theory			Experiment	Theory (MHz)	Theory (MHz)
K	J	F	Experimental	best fit	$g_A=-0.0132$		Field ($\pm.035g$)	(MHz)	best fit	$g_A=-0.00132$
1	$\frac{3}{2}$	2	0.4973(8)	0.4980	0.4989		269.260	18.857(60)	18.694	18.666
		1	0.8649(14)	0.8660	0.8661	$K=1$	271.750	14.930(42)	14.792	14.765
2	$\frac{5}{2}$	3	0.3308(4)	0.3306	0.3321	$J=\frac{3}{2}$	274.120	11.006(41)	11.085	11.059
		2	0.4701(6)	0.4712	0.4730	$F_1=2$	276.750	6.962(41)	6.979	6.955
3	$\frac{7}{2}$	4	0.2470(2)	0.2471	0.2486	$M_{F1}=-1$	281.610	−0.742(49)	−0.586	−0.607
		3	0.3214(2)	0.3212	0.3229	$F_2=1$	284.100	−4.497(26)	−4.451	−4.470
4	$\frac{9}{2}$	5	0.1971(2)	0.1971	0.1984	$M_{F2}=1$	286.600	−8.376(34)	−8.323	−8.341
		4	0.2427(3)	0.2428	0.2444		289.120	−12.222(34)	−12.219	−12.235
5	$\frac{11}{2}$	6	0.1637(2)	0.1638	0.1649		291.620	−16.023(47)	−16.076	−16.091
		5	0.1948(2)	0.1948	0.1961					
6	$\frac{13}{2}$	7	0.1400(1)	0.1400	0.1410					
		6	0.1627(1)	0.1624	0.1636		323.854	−12.050(45)	−11.959	−12.049
2	$\frac{3}{2}$	2	−0.3078(3)	−0.3075	−0.3118		327.406	−9.210(40)	−9.246	−9.312
		1	−0.4991(6)	−0.4985	−0.5062	$K=2$	329.656	−7.595(43)	−7.529	−7.579
3	$\frac{5}{2}$	3	−0.2416(2)	−0.2417	−0.2449	$J=\frac{3}{2}$	332.153	−5.650(53)	−5.625	−5.657
		2	−0.3336(2)	−0.3336	−0.3381	$F_1=2$	334.491	−3.822(35)	−3.844	−3.859
4	$\frac{7}{2}$	4	−0.1966(3)	−0.1971	−0.1995	$M_{F1}=-2$	337.129	−1.721(76)	−1.835	−1.832
		3	−0.2505(4)	−0.2510	−0.2541	$F_2=1$	344.551	3.766(33)	3.810	3.864
5	$\frac{9}{2}$	5	−0.1659(3)	−0.1660	−0.1679	$M_{F2}=0$	347.063	5.755(43)	5.718	5.789
		4	−0.2016(3)	−0.2013	−0.2037		349.632	7.738(38)	7.668	7.756
6	$\frac{11}{2}$	6	−0.1427(3)	−0.1432	−0.1448					
		5	−0.1681(3)	−0.1682	−0.1702					

In summary, errors in field measurements contribute little to our uncertainty.

The frequencies were measured by fitting to the data accumulated in the signal averager. In order to calibrate the time base, we injected a 2.0000-MHz signal into the input channel of the transient recorder. We found no corrections at the level of one part in 10^4.

Another possible source of systematic error arises from the model of quantum beats.[13,14,36] In particular, we have assumed that the laser pulse is spectrally white and temporally square, that the detection is polarization insensitive and temporally square, and that the optical geometry is truly orthogonal. Our calculations have shown the spectrum of the light and any geometrical misalignment can affect only the strength and phase of the signal, not its frequency. We tested the geometrical part of this calculation by comparing the fitted results of data sets taken with our best alignment with those from data sets taken with deliberately misaligned optics. We rotated the PMT optical axis by 10° and took four data sets on the $Q_1(2)$ line. The fitted parameters gave the same frequency to within 0.01% but the phase of the oscillations was changed from 332° and 295° to 370° and 345° in accordance with our expectations.

The pulse shape and light intensity have very little effect on our frequency measurements because the data are taken over a 2-μsec period long after the 7-nsec laser pulse is over. Any polarization sensitivity can only affect the signal-to-background ratio, and the nonsquare gate on the detection electronics that arises from our 10-nsec low-pass filter

can only alter the wave form but not change its frequency. Fourier analysis of our data shows no discernible evidence of this waveform distortion.

The optical measurement of the ρ-doubling constant γ is not nearly as free from systematic uncertainties. Although precautions were taken to assure uniform chart speed and grating rotation speed by using the clock motors, nonuniformities and buckling of the paper could result in a variety of errors. Therefore, we made a careful check of the linearity of the scan based on the rotational constant from Ref. 1 and found a small curvature. Although we corrected the wavelength scale by about 5% because of this, there still remain some possible effects. The shape and width of the laser spectrum have significant effect on the precision of this measurement, unlike the quantum-beat measurements. Although the spectrum in Fig. 6 is fairly symmetrical, it is not perfectly so. Small errors (5% of the linewidth) can arise from this asymmetry. We also considered the effect of the hfs of both ground and excited states. We found that its effect on the line shape and position was so small that neglecting it produced an error of less than 15 MHz in our result for γ. Of course, the best measurement of γ would come from a quantum-beat experiment, but it would require a field of many kG to bring two components of a ρ doublet within the bandwidth of our instruments. We are presently considering a microwave-optical quantum-beat measurement.

In summary, this experiment has been carefully designed so that systematic errors are of no consequence to the eventual precision. The accuracy of the numbers reported below is limited only by statistics, and could be improved by taking more data.

V. RESULTS

The results of our measurements are summarized along with previous work in Table II. The uncertainties we quote for the present work are derived solely from the statistical spread of the data as computed by the least-squares-fitting procedure. Our measured value for the spin-rotation constant γ is to be compared with the $X\,^2\Pi$ Λ-doubling constant p as discussed in Sec. III C and in the Appendix. The "unique perturber" approximation gives $\gamma=p$. The experimental value ($\Gamma=6862\pm42$ MHz) is less than the p value obtained from a combined optical and microwave data fit ($p=7039$ MHz) but once the difference of the perturbation sums is considered (Tables III and IV) the expected value of γ becomes 6564 MHz, suggesting that higher-lying states contribute $\sim4\%$. A fit of p from purely optical data[39] ($p=7375$ MHz) yields $\gamma=6877$ MHz, just outside our experimental error. We conclude that the method of fitting the ground-state parameters needs to be carefully considered in attempting to carry the two-state model beyond 5% accuracy. Furthermore, when r dependence in $T(AL)$ and $T(L)$ is considered, the electronic part cannot be factored out of the sums over v or v'' [Eqs. (13) and (A21)]. Recent *ab initio* calculations indicate that $T(AL)$ decreases with r so as to further decrease the ratio γ/p by $1-2\%$.

The present values for the hfs constants are close to those reported by ter Meulen *et al.*[11] differing by just slightly more than the combined error limits. Values from configuration-interaction (CI) calculations and from many-body perturbation theory are surprisingly close to the experimental values.

The experimental value for g_r in Table II is, to our knowledge, the first measurement of a rotational g factor for a molecular $^2\Sigma$ state, and the first for a nonmetastable excited state. The experimental value agrees with our theoretical estimate based simply on coupling with $X\,^2\Pi$. The agreement with the theoretical value definitely confirms that the sign of the electron contribution is the same as that of the nuclear contribution. All previous measurements of molecular g_r values, primarily from $X\,^1\Sigma^+$ ground states, have yielded an electron contribution that is opposite in sign to the nuclear contribution, as would be expected for a rotating cloud of particles of opposite charge. A positive value for g_{er}, which suggests that the electrons rotate "backwards," obliges one to revise the traditional point of view that takes the magnetic moment associated with a "rigid" cloud of electrons as "normal" and attributes the normally smaller (negative) observed values as being due to "slip" of the electrons around the rotating nuclei. In fact, it has long been known[31,42] that the first-order contribution to g_r from electron motion arising from the $\vec{B}\cdot\vec{L}$ term is zero diagonally within a Σ state. The primary effect of molecular rotation is to introduce Coriolis effects because angular momentum along the internuclear axis is no longer conserved. In Σ states, g_{er} arises from a mixture of Π character and therefore the sign of the effect depends on whether the predominantly coupled Π state is above or below the observed Σ state.

Our experimental value of g_{er} $(=g_r-g_{Nr})$ $=0.001\,95(6)\mu_B$, is more than 25 times the magni-

TABLE II. Parameter values of the $A\,^2\Sigma^+$ state of OH. The values shown here compare our results (labeled d) with several others.

γ: ρ-doubling constant	
Optical spectrum analysis (expt)	6732 MHz [a]
Reanalysis of optical data (expt)	6930±72 MHz [b]
Molecular-beam–laser spectroscopy (expt)	7130±30 MHz [c]
Quantum-beat spectroscopy (expt)	6862±43 MHz [d]
Calculated from A-X coupling (theory)	6564 MHz [d]
$b+c/3$: Fermi-contact part of hfs	
Level crossing in OD ($v=0$), restated for proton moment (expt)	769±46 MHz [e]
Molecular-beam–laser spectroscopy (expt)	777.8±2.0 MHz [c]
Quantum-beat spectroscopy (expt)	774.1±0.4 MHz [d]
Many-body perturbation theory (theory)	750 MHz [f]
CI calculation, including vibrational averaging for OH $v=0$ (theory)	792 MHz [g]
c: hfs constant	
Level crossing in OD ($v=0$), restated for proton moment (expt)	143±91 MHz [e]
Molecular-beam–laser spectroscopy (expt)	165.8±2.8 MHz [c]
Quantum-beat spectroscopy (expt)	168.9±0.8 MHz [d]
CI, vibrationally averaged for OH $v=0$ (theory)	164.2 MHz [g]
g_r: Rotational g factor	
Quantum-beat spectroscopy (expt)	$(2.46\pm0.06)\times10^{-3}\,\mu_B$ [d]
$g_{Nr}+g_{er}$ from A-X coupling (theory)	$2.42\times10^{-3}\,\mu_B$ [d]
g_A: Anisotropic g factor	
Quantum-beat spectroscopy (expt)	$(2.42\pm0.11)\times10^{-2}\,\mu_B$ [d]
Calculated from A-X coupling (theory)	$-1.30\times10^{-2}\mu_B$ [d]

[a]Reference 1.
[b]Reference 39.
[c]Reference 11.
[d]This work.
[e]Reference 10.
[f]Reference 40.
[g]Reference 41.

tude of g_{er} for H_2 $X\,^1\Sigma_g^+$, and about four times the magnitude of the largest value of g_{er} computed from Mizushima's Tables 4–9.[34] This is because the OH state is open shell, coupled in pure precession with the $X\,^2\Pi$ state. As Foley[43] noted some time ago, matrix elements of $\langle \Pi \mid L_+ \mid \Sigma \rangle$ are expected to be smaller for closed-shell Σ states where pure-precession coupling does not take place. Quite

clearly, experimental g_{er} values for excited states offer interesting probes of interstate coupling elements to be compared with other studies of perturbation effects.

The parameter g_A differs substantially from the theoretical value, which takes into account only coupling with $X\,^2\Pi$. In contrast to the Coriolis terms contained in g_{er}, the spin-orbit coupling terms in g_A may be expected to couple with $^2\Pi$ states not in a "pure-precession" relation to the $^2\Sigma$ state, so the neglect of other $^2\Pi$ states is less valid for the g_A parameter. We have tried fixing its value in a series of least-squares fits to the other parameters, but there is a strong coupling between g_A and c that distorts the results significantly. Also, the fit to the data is noticeably worse (see Fig. 7). We cannot obtain agreement between theory and experiment for g_A and do not know why. Our results for the smaller quantity g_r are better because of its different dependence on angular momenta and consequent decoupling from the other parameters.

We have tried to introduce a term $a\vec{I}\cdot\vec{J}$ into the Hamiltonian matrix in the fitting program. We found a very high degree of correlation with the hyperfine parameters b and c so that a cannot be determined independently. Fixing a at 0.4 MHz (theoretical estimate) resulted in displacements of b and c about equal to our quoted experimental error in each. Since this effect is uncorrelated with the experimental data spread, the errors for "true" parameters b and c would be about $\sqrt{2}$ the values quoted in Table II.

We have considered the use of time-delayed spectroscopy in order to achieve higher precision[44] but it would not improve the results reported here. Although each individual data fit returns frequencies accurate to about $\frac{1}{4}$ the natural width, the ultimate precision of our results is not limited by this uncertainty. Instead it derives from the statistical scatter of the least-squares fit that determines the molecular parameters from our measured frequencies. Since the accuracy of the experiment is not limited by possible unknown systematic errors, but by the scatter in the results, time delayed line narrowing would not improve the precision.[44] Only significantly more data can reduce the uncertainties to less than the natural width of 0.22 MHz so that line-narrowing techniques might be considered. In view of the unusual immunity of these measurements from systematic errors however, major improvements in data acquisition would be required to reach this level of precision.

In summary, we have developed a new application of quantum beats to make precision measurements in the vicinity of level crossings and have used it to determine hfs constants and g factors of excited molecular states to unprecedented accuracy. The resulting hfs constants are in good agreement with previously measured values[11] but are much more accurate. We have developed a model Hamiltonian whose eigenvalues are in excellent agreement with our measurements.

ACKNOWLEDGMENTS

We thank Pat McNicholl and Tom Abbruzzese for help in some of the data taking. We gratefully acknowledge the support of the National Science Foundation.

APPENDIX

The parameters γ, g_{er}, and g_A measured here may also be calculated. We use a model that assumes that only coupling between the A and X states is significant for all r values of interest. Other electronic states are much higher and more weakly coupled, so that this approximation is reliable to within a few percent.[9] Better measurements require this model to be examined in more detail. In this appendix, we give parameters used to evaluate the sums over vibrational levels that occur in

TABLE III. Vibrational overlap integrals and energy denominators used in evaluating perturbation sums.

v_A, v_X	$\langle v_A \mid v_X \rangle$	$\langle v_A \mid B_r \mid v_X \rangle / \langle v_A \mid v_X \rangle$	$E(Av_A) - E(Xv_X)$
0,0	0.950 25	17.758 cm^{-1}	32 402.0 cm^{-1}
0,1	0.306 03	9.236	28 832
0,2	0.057 56	9.031	25 430
1,0	−0.297 67	24.881	35 389
2,0	0.087 10	34.910	38 182

TABLE IV. Perturbation sums occurring in various parameters.

Summation	In parameter	Equation no.	Value
$\sum_v \langle v \mid B_r \mid v'' \rangle \langle v'' \mid v \rangle / D(v,v'')$	$p(^2\Pi)$	(A1)	-5.634×10^{-4}
$\sum_v \mid \langle v \mid B_r \mid v'' \rangle \mid^2 / D(v,v'')$	$q(^2\Pi)$	(A2)	-1.057×10^{-2}
$\sum_{v''} -\langle v \mid B_r \mid v'' \rangle \langle v'' \mid v \rangle / D(v,v'')$	$\gamma(^2\Sigma), g_{er}(^2\Sigma)$	(13) and (19)	5.254×10^{-4}
$\sum_{v''} - \mid \langle v \mid v'' \rangle \mid^2 / D(v,v'')$	$g_A(^2\Sigma)$	(17)	3.12×10^{-5}
$D(v,v'') = E(^2\Pi v'') - E(^2\Sigma v)$			

Eqs. (13), (17), and (19) for comparison with the $X\,^2\Pi$ parameters

$$p = 4\langle 0||T^1_{-1}(L)||1\rangle\langle 1||T^1_1(AL)||0\rangle \times \sum_v \frac{\langle v \mid B_r \mid v''\rangle\langle v'' \mid v\rangle}{E(^2\Pi^+ v'') - E(^2\Sigma v)} \tag{A1}$$

and

$$q = 4 \mid \langle 0||T^1_{-1}(L)||1\rangle \mid^2 \sum_v \frac{\mid \langle v \mid B_r \mid v'' \rangle \mid^2}{E(^2\Pi v'') - E(^2\Sigma v)} \cdot \tag{A2}$$

We have computed the necessary overlap integrals by numerical integration of RKR potentials and present the results in Table III. The summations are given in Table IV.

In a recent comprehensive analysis of OH optical and microwave data, p and q were not fit directly, but the $A\,^2\Sigma^+$ ($v=0$) level was included in the Hamiltonian matrix so that $T^1_1(L)$ and $T^1_1(AL)$ could be fitted. This assumed that coupling only between $v=0$ levels of the A and X states occurs, so the sums in (A1) and (A2) reduce to one term. To go beyond this restrictive assumption, we use the full summations (Table IV), the data of Table III, $q=0.238$ cm^{-1} and $p=0.236$ cm^{-1} (from Table III of Ref. 31) to extract the new values $T^1_1(L)=0.949$ and $T^1_1(AL)=-108.97$ cm^{-1}. These values are then used to compute estimates for γ, g_{er}, and g_A.

Although the energy denominators for v or $v''\neq0$ are larger in the expression for p than for γ, note that γ is actually less than p because $\langle v \mid R^{-2} \mid v''\rangle$ increases with v for $v''=0$, but decreases with v'' for $v=0$ (Table III).

*Present address: Department of Physics, University of Physics, University of Washington, Seattle, Washington 98195.

[1]G. Dieke and H. Crosswhite, J. Quant. Spectrosc. Radiat. Transfer 2, 97 (1962).
[2]W. L. Meerts and A. Dymanus, Can. J. Phys. 53, 2123 (1975); Astrophys. J. 187, L45 (1974).
[3]H. E. Radford, Phys. Rev. 122, 114 (1961); 126, 1035 (1962).
[4]P. R. Clough, A. H. Curran, and B. A. Thrush, Proc. R. Soc. London Ser. A 323, 541 (1971).
[5]K. M. Evenson, J. S. Wells, and H. E. Radford, Phys. Rev. Lett. 25, 199 (1970); M. Mizushima, Phys. Rev. A 5, 143 (1972); J. M. Brown, M. Kaise, C. M. L. Kerr, and D. J. Milton, Mol. Phys. 36, 553 (1978).
[6]A. Marshall, R. L. de Zafra, and H. Metcalf, Phys. Rev. Lett. 22, 445 (1969).
[7]K. R. German and R. N. Zare, Phys. Rev. Lett. 23, 1207 (1969); Phys. Rev. 186, 9 (1969).
[8]R. de Zafra, A. Marshall, and H. Metcalf, Phys. Rev. A 3, 1557 (1971).
[9]K. R. German, T. H. Bergeman, E. M. Weinstock, and R. N. Zare, J. Chem. Phys. 58, 4304 (1973).
[10]E. M. Weinstock and R. N. Zare, J. Chem. Phys. 58, 4319 (1973).
[11]J. Termeulen, G. van Mierlo, and A. Dymanus, Phys. Rev. Lett. 43, 29 (1979).
[12]D. H. Phelps and F. W. Dalby, Can. J. Phys. 43, 144 (1965); E. A. Scarl and F. W. Dalby, *ibid.* 49, 2825 (1971).
[13]F. J. Raab, T. H. Bergeman, D. Lieberman, and H. Metcalf, Opt. Lett. 5, 427 (1980).
[14]P. Lebow, F. Raab, and H. Metcalf, Phys. Rev. Lett. 42, 85 (1979).
[15]J. H. Brophy, J. A. Silver, and J. L. Kinsey, Chem. Phys. Lett. 28, 418 (1974); W. L. Dimpfl and J. L. Kinsey, J. Quant. Spectrosc. Radiat. Transfer 21, 233 (1979).
[16]R. K. Lengel and D. R. Crosley, Chem. Phys. Lett. 32, 261 (1975); D. R. Crosley and G. P. Smith, Appl.

Opt. 19, 517 (1980).
[17]D. Stepowski and M. Cottreau, Appl. Opt. 18, 354 (1979).
[18]P. Hogan and D. Davis, Chem. Phys. Lett. 29, 555 (1974).
[19]C. C. Wang and L. I. Davis, Phys. Rev. Lett. 32, 349 (1974); C. C. Wang *et al.*, Science 189, 797 (1975); C. C. Wang and D. K. Killinger, Phys. Rev. A 20, 1495 (1979).
[20]W. S. Heaps, Appl. Opt. 19, 243 (1980).
[21]C. Chan and J. Daily, Appl. Opt. 19, 1963 (1980).
[22]K. R. German, J. Chem. Phys. 62, 2584 (1975).
[23]A. B. Meinel, Astrophys. J. 111, 433 (1950); 111, 555 (1950); 112, 120 (1950); and references therein.
[24]B. Weinstock and H. Niki, Science 176, 290 (1972). See also Refs. 11 and 20.
[25]P. Schenck and H. Metcalf, Appl. Opt. 12, 183 (1973); M. Feldman, P. Lebow, F. Raab, and H. Metcalf, Appl. Opt. 17, 774 (1978).
[26]R. Wallenstein and T. Hansch, Opt. Commun. 14, 353 (1975).
[27]A. H. Firester, Rev. Sci. Instrum. 37, 1264 (1966).
[28]R. Frosch and H. Foley, Phys. Rev. 88, 1337 (1952).
[29]H. Radford, Phys. Rev. A 136, 1571 (1964).
[30]A. R. Edmonds, *Angular Momentum in Quantum Mechanics* (Princeton University Press, Princeton, New Jersey, 1957).
[31]L. Veseth, J. Mol. Spectrosc. 59, 51 (1976); 63, 180 (1976); 66, 259 (1977).
[32]A. Jordahl, Phys. Rev. 45, 87 (1934).
[33]J. L. Destombes, C. Marliere, and F. Rohart, J. Mol. Spectrosc. 67, 93 (1977).
[34]M. Mizushima, *The Theory of Rotating Diatomic Molecules* (Wiley, New York, 1975).
[35]A. Carrington, D. Levy, and T. Miller, Adv. Chem. Phys. XVIII, 149 (1970).
[36]P. Schenck, R. Hilborn, and H. Metcalf, Phys. Rev. Lett. 31, 189 (1973).
[37]L. J. Curtis and P. Erman, J. Opt. Soc. Am. 67, 1218 (1977).
[38]J. Brzozowski, P. Erman, and M. Lyyra, Phys. Scr. 17, 507 (1978).
[39]E. A. Moore and W. G. Richards, Phys. Scr. 3, 223 (1971).
[40]J. E. Rodger and T. P. Das, Phys. Rev. A 8, 2195 (1973).
[41]S. Green, J. Chem. Phys. 58, 4327 (1973).
[42]G. C. Wick, Z. Phys. 85, 25 (1933); Phys. Rev. 73, 51 (1948).
[43]H. M. Foley, Phys. Rev. 72, 504 (1947).
[44]H. Metcalf and W. Phillips, Opt. Lett. 5, 540 (1980).